Multiparameter Single Sensor for Space Silicone Adhesive Monitoring Under High-Vacuum Ultraviolet Exposure

Fazzi, Luigi; Dias, Nuno; Holynska, Malgorzata; Tighe, Adrian P.; Rampini, Riccardo; Groves, Roger M.

DOI
10.2514/1.A35531

Publication date
2023

Document Version
Final published version

Published in
Journal of Spacecraft and Rockets

JOURNAL OF SPACECRAFT AND ROCKETS
Vol. 60, No. 3, May–June 2023

Multiparameter Single Sensor for Space Silicone Adhesive Monitoring Under High-Vacuum Ultraviolet Exposure

Luigi Fazzi*
Delft University of Technology, 2629 HS Delft, The Netherlands
Nuno Dias,† Malgorzata Holynska,‡ Adrian P. Tighe,‡ and Riccardo Rampini§
ESA, 2200 AZ Noordwijk, The Netherlands
and
Roger M. Groves¶
Delft University of Technology, 2629 HS Delft, The Netherlands

https://doi.org/10.2514/1.A35531

Tilted fiber Bragg grating (TFBG) sensors were demonstrated to simultaneously measure the material thermomechanical and refractometric state in which they are embedded. In this work, for the first time, TFBGs are investigated for three-parameter monitoring of space-qualified NuSil® CV16-2500 silicone operating during high-vacuum ultraviolet (UV) exposure. The first part of the work is focused on the ultraviolet effect on the TFBG spectrum when the sensor is 1) directly exposed to the radiation, 2) covered by a thin cover glass, and with a Kapton layer on top. Successively, the silicone is used as an adhesive in a sandwich structure in which the TFBGs are embedded and exposed under high vacuum to various UV/vacuum UV intensity radiations and durations. The sensors' spectra were acquired and demodulated to detect the silicone strain–temperature–refractive index variations and correlate the silicone refractometric changes with the equivalent exposure solar hours. The second part of the paper is on silicone degradation state evaluation using the same sensor but during a direct exposure of the adhesive to the radiation. This allowed the UV effects on the silicone to be enhanced but needed a method to compensate for the damaging effect of UV radiation on the TFBG spectrum.

Nomenclature

A	=	noncompensated area value
A_{new}	=	compensated envelope area
A_{var}	=	variation of the envelope area
a	=	coefficient of the linear parameter
b	=	known coefficient of the linear fitting
K	=	global thermomechanical sensitivity matrix
$k_{T_{\text{Bragg}}}$	=	thermal sensitivity coefficient of the Bragg peak, $\text{pm}/^\circ\text{C}^{-1}$
$k_{T_{\text{ghost}}}$	=	thermal sensitivity coefficient of the ghost peak, $\text{pm}/^\circ\text{C}^{-1}$
$k_{\varepsilon_{\text{Bragg}}}$	=	strain sensitivity coefficient of the Bragg peak, $\text{pm}/\mu\varepsilon^{-1}$
$k_{\varepsilon_{\text{ghost}}}$	=	strain sensitivity coefficient of the ghost peak, $\text{pm}/\mu\varepsilon^{-1}$
P	=	percentage of the NuSil transmission, %
P_{Area}	=	unitary envelope area decay
P_a	=	compensated unitary envelope area variation
P_{com}	=	compensated unitary decay of the envelope area
P_{var}	=	decay variation of the NuSil transmission
t	=	time, h
ΔT	=	variation of the temperature, °C
$\Delta\varepsilon$	=	variation of the mechanical deformation, $\mu\varepsilon$
$\Delta\lambda_{\text{Bragg}}$	=	variation of the wavelength of the Bragg peak, nm
$\Delta\lambda_{\text{ghost}}$	=	variation of the wavelength of the ghost peak, nm
θ	=	tilt angle of the tilted fiber Bragg grating, deg

Received 25 July 2022; revision received 25 October 2022; accepted for publication 6 November 2022; published online 30 January 2023.

*Ph.D. Researcher, Aerospace Structures and Materials Department, Aerospace Non-Destructive Testing Laboratory, Structural Integrity and Composites Group, Faculty of Aerospace Engineering; also Visiting Researcher, ESA, European Space Research and Technology Center, Technology, Engineering and Quality—Quality Evaluation Engineering (TEC-QEE), Keplerlaan 1, 2200 AZ Noordwijk, The Netherlands.

†Materials Engineer, European Space Research and Technology Center, TEC-QEE, Keplerlaan 1.

‡Materials and Process Engineer, European Space Research and Technology Center, TEC-QEE, Keplerlaan 1.

§Head of TEC-QEE Section, European Space Research and Technology Center, TEC-QEE, Keplerlaan 1.

¶Associate Professor, Aerospace Structures and Materials Department; Head of the Aerospace Non-Destructive Testing Laboratory, Structural Integrity and Composites Group, Faculty of Aerospace Engineering.

I. Introduction

IN ONE of our previous works [1], the effects of thermal cycles in high vacuum on NuSil CV16-2500 were studied by embedding a special three-parameter optical fiber (OF) sensor called a tilted fiber Bragg grating (TFBG) in the silicone adhesive of a cover glass sandwich sample. The aim was to detect the thermomechanical and possibly chemical evolutions in the elastomer via the simultaneous strain–temperature–refractive-index measurements performed by the single TFBG sensor when the material was exposed to a simulated space environment characterized by high-vacuum thermal cycles. In this work, the harsh space environment was simulated by creating a high vacuum and exposing several samples to ultraviolet (UV) radiation at different intensities (expressed in number as solar constants) and for several exposure times. Hence, the silicone samples underwent not only vacuum and high temperatures but also to UV radiation. Indeed, although space-qualified silicones have been studied and developed for many years to be resistant to the harsh space working conditions, they must coexist with ultra-high-vacuum, ultraviolet, and ionizing radiations; extreme thermal ranges and cycles; thermal shock; microgravity; atomic oxygen (ATOX); high accelerations; vibrations; and space debris for their entire functional lives. The combination of these effects may cause severe damage and decreasing mechanical performance, changing of the original material properties, and even premature failure of the components [2].

UV radiation is particularly dangerous for polymers (silicones included) because the organic chemical composition is photochemically susceptible to degradation at light wavelengths between 200 and 400 nm [3]. Indeed, organic molecules absorb UV light, initiating photochemical reactions that cause the rupture of the original bonds. The radical reactions released due to the cleavage of homolytic bonds

induce discoloration of the transparent silicones, with the unwanted consequence of producing a much stronger solar absorbance capability. This effect is especially high when volatiles are released and nonsaturated bonds are present in the remaining material, or even if there are impurities contained in the polymer. All these effects will increase the absorption of UVs contributing to the photochemical reactions [4–6]. Apart from the discoloration/coloration, this degradation process changes the original thermo-optical properties and efficiency, as well as decreases the silicone mechanical performance and durability. Even worse consequences may occur when UV effects are combined concurrently with other space phenomena: in particular, microcracking, severe degradation, and premature failures [2–6]. In addition, ultrahigh vacuum can affect the original dimensional stability and composition of the polymer because it induces silicone outgassing of additives and low-molecular-weight residues. In this way, contaminant layers may deposit on nearby cold surfaces; and their interaction with UV or ionizing radiation, thermal cycles, and ATOX can induce their fixation. This might compromise quality or efficiency, or even cause severe issues [7].

Therefore, taking into account these harsh operational conditions and the consequences of their combined actions on the materials, the materials and the components for space flight undergo strict development, qualification, acceptance, and protoflight-test campaigns to verify and certify their suitability for space applications, to evaluate their degradation state after the space environment exposure, and to minimize the risk of premature failure [8]. However, testing campaigns are very time consuming and expensive in terms of resources, equipment, apparatuses, and personnel; so, intermediate verification methods are necessary to estimate the sample condition. Hence, with the evolution of the space industry, several nondestructive evaluation techniques have been developed to monitor the health state of the materials during ground testing and in service [9–14]. However, although many technologies might be used for in situ evaluation/remote/real-time monitoring [15], the sensors and the support apparatus must match the space compatibility [16] and embedding requirements [17]. Another issue is in regard to the need to perform multiparameter measurements to evaluate the overall state of a material or for simple cross-sensitivity compensation of some sensors to a determined parameter (as in the case of temperature for strain gauges). This involves the integration of more sensors inside the materials and apparatuses in the spacecraft, with a consequent increase of the weight and complexity of the overall system, costs, and reduction of the volume available for the payload.

TFBG sensors address these issues by being minimally intrusive and able to simultaneously measure many parameters such as strain–temperature and refractive index (RI) variations [18]. In the previous work by Fazzi et al., the TFBG sensor was demonstrated to be compatible with vacuum applications. In this new work, some TFBGs were preliminary tested under high-vacuum UV exposure to investigate possible material degradation. Then, the TFBGs were embedded inside the silicone adhesive of the cover glass sandwiches to evaluate the thermomechanical and refractometric states of the elastomer. Specifically, the TFBG was embedded inside the silicone elastomer, which acted as an adhesive layer between two glass plates, in a sandwichlike structure where the core was made of silicone and the faces were glass plates. Of particular interest is the RI trend as the equivalent solar hours (ESHs) of exposure to the UV light are increased. Therefore, in summary, the TFBG sensor has already been demonstrated as a potential sensor for space applications that can perform reliable and multiparameter measurements, which provide important information on the material state and will be investigated further in this paper.

II. TFBG Sensing Theory

The special features of TFBG sensors allow the use of their different peaks in the transmitted spectrum to be used for simultaneous strain–temperature variation detection and refractometric measurements. A TFBG sensor is obtained by imposing a permanent modulation of the RI inside the core of a single-mode optical fiber [19]. However, unlike a standard fiber Bragg grating (FBG), the modulation is tilted at a certain angle (called the tilt angle θ) with respect to the optical axis of the fiber. The slanted Bragg gratings enhance the coupling between the modes, propagating in the cladding layer and backreflected into the core of the OF. Especially for a weakly tilted FBG ($\theta < 10$ deg), this coupling system supports three kinds of resonance peaks in the transmission spectrum, which are called the Bragg, ghost, and cladding peaks [19]; see Fig. 1.

The Bragg peak is generated by the coupling between the forward- and backward-propagating core modes, whereas the ghost mode comes from a congregation of multiple peaks placed at (approximately) the same wavelength, which are confined and interacting at the interface of the internal OF layers [19]. The Bragg and ghost peaks are selected here to perform the measurements of the strain and temperature variations inside the silicone adhesive. The demodulation technique is based on a sensing matrix composed of the thermomechanical sensitivity coefficients of the selected peaks that, when multiplied by the wavelength shift variations of the selected peaks, returns the variations of the strain $\Delta\varepsilon$ and temperature ΔT. The procedure is represented in [20]

$$\begin{bmatrix} \Delta\varepsilon \\ \Delta T \end{bmatrix} = \begin{bmatrix} k_{\varepsilon_{\text{Bragg}}} & k_{T_{\text{Bragg}}} \\ k_{\varepsilon_{\text{ghost}}} & k_{T_{\text{ghost}}} \end{bmatrix}^{-1} \begin{bmatrix} \Delta\lambda_{\text{Bragg}} \\ \Delta\lambda_{\text{ghost}} \end{bmatrix} = [\text{K}]^{-1} \begin{bmatrix} \Delta\lambda_{\text{Bragg}} \\ \Delta\lambda_{\text{ghost}} \end{bmatrix} \quad (1)$$

where $k_{\varepsilon_{\text{Bragg}}}$, $k_{\varepsilon_{\text{ghost}}}$, $k_{T_{\text{Bragg}}}$, and $k_{T_{\text{ghost}}}$ are, respectively, the strain and thermal sensitivity coefficients of the Bragg and ghost peaks; whereas $\Delta\lambda_{\text{Bragg}}$ and $\Delta\lambda_{\text{ghost}}$ are their wavelength shifts due to the positive or negative thermomechanical perturbations. The sensitivity coefficients can be obtained by calibration as reported in Ref. [20]. The nonsusceptibility of the Bragg and ghost peaks to the external RI variations allows three-parameter measurements with a single TFBG [19,21]. For the TFBGs used in this work, the following sensitivity coefficients were determined using the method described in Ref. [20]: $k_{\varepsilon_{\text{Bragg}}} = 1.225 \pm 0.004$ pm/$\mu\varepsilon$, $k_{\varepsilon_{\text{ghost}}} = 1.225 \pm 0.006$ pm/$\mu\varepsilon$, $k_{T_{\text{Bragg}}} = 8.959 \pm 0.223$ pm/°C, and $k_{T_{\text{ghost}}} = 9.235 \pm 0.275$ pm/°C. The thermal resolution (TR) is approximately 7°C.

The cladding resonance peaks in the spectrum shown in Fig. 1 can be used to evaluate the RI of the medium surrounding the sensor. This measurement is achieved by first performing a preliminary calibration of the TFBG by immersing it in liquids that have a well-defined RI (accuracy ±0.0002). At each immersion, an envelope of the upper and lower cladding peaks is made so that the envelope area can be calculated and later normalized with respect to a reference area. The reference area is an arbitrary envelope area among those obtained during the RI calibration; in this case, it was selected as the maximum area (corresponding to the immersion in 1.33 RI liquid). The envelope area calculation can be performed with different techniques; however, here, we apply a recently developed technique based on Delaunay triangulation (D-T) [19]. All the details regarding the calibration setup, procedure, specifications, and the D-T demodulation technique can be consulted in the same reference [19]. Once the

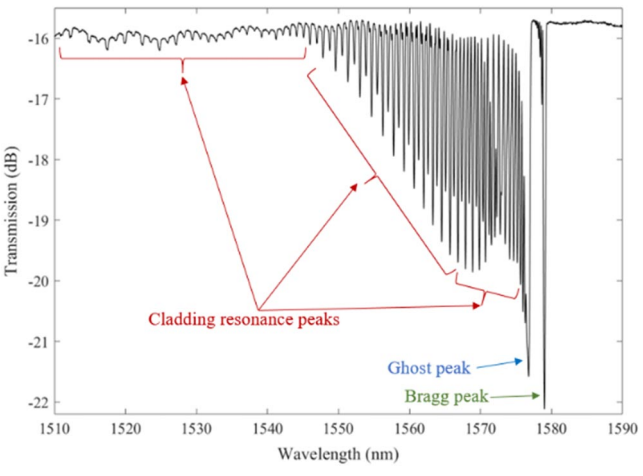

Fig. 1 Transmission spectrum of a 3 deg TFBG.

refractometric calibration curve has been obtained, a fitting function is extracted based on the RI working range. From this point, the TFBG is able to measure the external RI because the fitting function can be solved with respect to the envelope area value obtained from the spectrum of the immersed sensor. A more detailed analysis of a refractometric performance of the TFBG has been reported in Ref. [21]. Once the thermomechanical and refractometric calibrations are completed, the TFBG is ready to be embedded in the polymer.

To achieve a proper and complete investigation of the UV effects on the silicone adhesive through the three-parameter measurements performed by the embedded TFBGs, the experimental campaign has been divided into three different parts. First of all, the TFBG is tested under UV light to investigate the effects of the radiation on the spectrum of the sensor. In the second part, samples composed of cover glasses and silicone adhesives are prepared with embedded TFBGs and a K-type thermocouple (TC). The third experiment investigates the aging in the silicone due to UV exposure when the cover glass is not blocking the radiation.

III. Samples

The first group of samples includes bare TFBGs where the OF coating has been removed in the region of the sensor. The bare TFBGs were 1) tested under direct exposure to UV light, 2) covered by a thin cover glass, and 3) covered by a thin Kapton® layer. The aim of these measurements is to prove that the sensor works as intended and to confirm its reliability in the specified working conditions. These samples were tested in high vacuum with increasing ESH values of UV exposure. TFBG spectra were recorded to investigate the thermomechanical and refractometric states of the silicone adhesive, and a compensation procedure was performed on the TFBG spectrum to obtain the real RI value of the aged silicone.

Descriptions of the samples used during the testing campaigns are presented in this section. For this experiment, three TFBGs were used. The first one was directly exposed to the UV radiation (Fig. 2, point a), the second was covered by a layer of cerium doped microsheets of cover glass ($30 \times 20 \times 0.05$ mm) (Fig. 2, point b), and the third was exposed but protected by a layer ($\sim$200 μm) of Kapton foil (Fig. 2, point c). All the TFBGs had a TC placed as close as possible.

The second type of sample includes the cover glass sandwiches sensorized with TFBGs and TCs. Each sample is composed of two layers of cerium doped microsheets of cover glass ($30 \times 20 \times 0.05$ mm) bonded together with the silicone adhesive NuSil CV16-2500 in which a bare TFBG sensor and a TC are embedded. The dimensions of the samples and the embedding distances of the sensors are reported in Fig. 3.

The last sample is composed of similar components of the second experiment but the cover glass on one of the sides is removed to directly expose the silicone to the UV radiation. The details of this sample are reported in Fig. 4.

IV. Equipment

All the TFBG sensors used in this work were manufactured by FORC-Photonics in Fibercore PS 1250/1500 OF by using the rotated phase-mask technique. All the sensors have a 3 deg tilt angle and are 4 mm long. The sensors are uncoated for approximately 20 mm of length, and the remaining OF is coated by a layer of UV-cured acrylate. The TFBGs were certified by the manufacturer to operate in a temperature range between −40 and 250°C without degradation of the spectrum for long exposure times (more than 720 h). The K-type

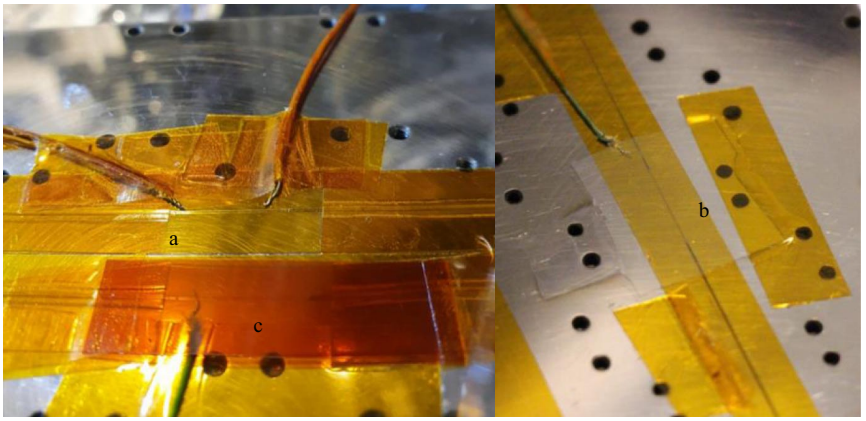

Fig. 2 Photographs of bare TFBG (point a), TFBG with cover glass (point b), and Kapton layer (point c).

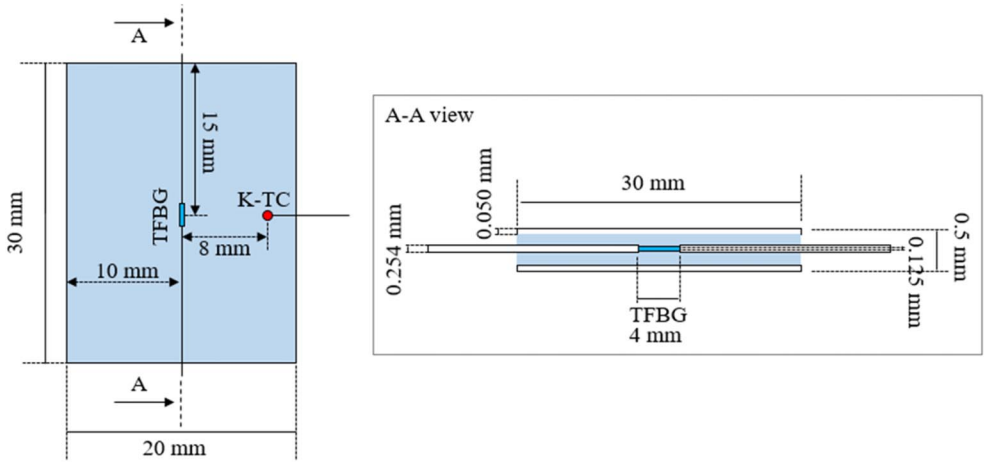

Fig. 3 Schematic of the sensorized cover glass sandwich samples.

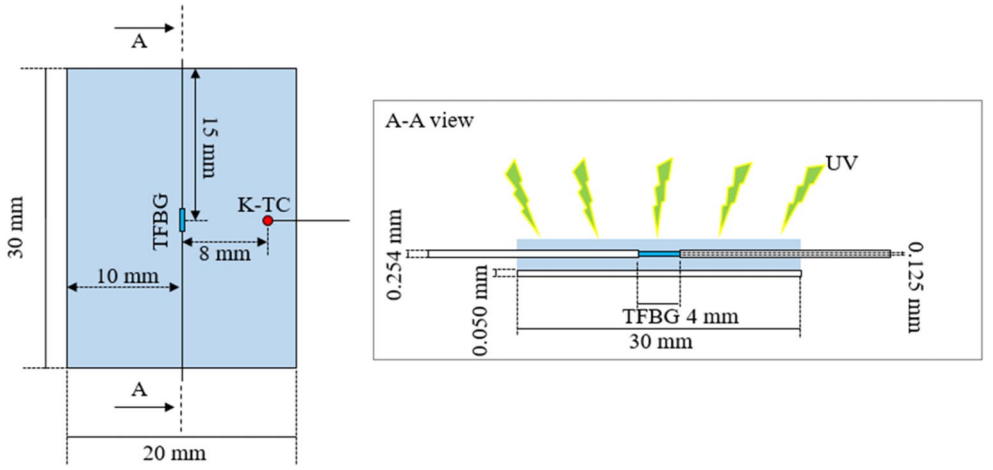

Fig. 4 Schematic of the sensorized assembly of cover glass and silicone adhesive.

TCs used have a diameter of ~200 μm and ± 1°C of accuracy. Before embedding of the sensors, a preliminary thermomechanical and refractometric calibration was performed on the TFBGs in order to obtain the sensitivity coefficients of Eq. (1) as well as the fitting correlation function between the envelope area and the surrounding RI. The TFBGs were calibrated before testing, as introduced in Sec. II. During the entire calibration and testing stage, the TFBG spectra were always acquired by using the National Instruments PXI-4844 interrogator (scanning wavelength resolution = 4 pm, scanning accuracy = ± 1 pm, and minimum power detection = 6.103×10^{-4} dB · m). The sensing system apparatus was provided by the Aerospace Non-Destructive Testing Laboratory of Delft University of Technology, whereas the high-vacuum UV radiation tests were performed using the MCross facility at the Materials and Electrical Components Laboratory of the ESA's European Space Research and Technology Center.

The MCross (Fig. 5a) is a vacuum chamber provided with an Agilent scroll pump and a Pfeiffer turbomolecular vacuum pump with a TC360 electronic drive unit (vacuum better than 10^{-5} mbar), two vacuum UV (VUV) deuteria, and two high-pressure discharge UV lamps (reaching a maximum of six solar constants). Inside the test chamber, a metallic sample plate (Fig. 5b) was placed on top of a resistance heating plate (Thermocoax), which was mounted on a liquid nitrogen coolable plate. The chamber was also equipped with Kapton-coated K-type TCs, which could be attached to the sample or the plate for temperature monitoring. In order to acquire the spectra of the OF sensors, the facility was also upgraded with two hermetic polarization-maintaining fiber optic feedthroughs manufactured by SQS, each of which had two input/output FC/APC connectors, externally connected with two optical circulators, and hence to the interrogator system. Before each test, the UV intensity (in solar constant) was measured at different sample positions. The solar constant is an internationally recognized unit used to unequivocally quantify the intensity of electromagnetic radiation that falls on a unit area of surface normal to the line from the sun at 1 astronomical unit (AU), outside the atmosphere, per unit time [22]. Specifically, the solar flux mean value at 1 AU is defined as 1366.1 W/m^2, which corresponds to one solar constant. This value can be measured on the surface of the support plate in correspondence with the sample positions through a UVpad spectral radiometer (Opsytec Dr. Gröbel), which measures the radiation intensity in the UVA (315–400 nm), UVB (280–315 nm), and UVC (100–280 nm) wavelengths. These values are converted to solar constants [22]. This value is then multiplied by the exposure time to obtain the ESH, which is the acceleration factor.

V. UV Effects on the TFBG Sensors

In this section, the effects of the UV radiation on the TFBG spectrum are treated. Indeed, because the TFBGs are made by inducing a modulation of the core RI with UV light interference, an external UV radiation incident on the photosensitive silica layers of the not-recoated OF may modify the RI profile imposed during the

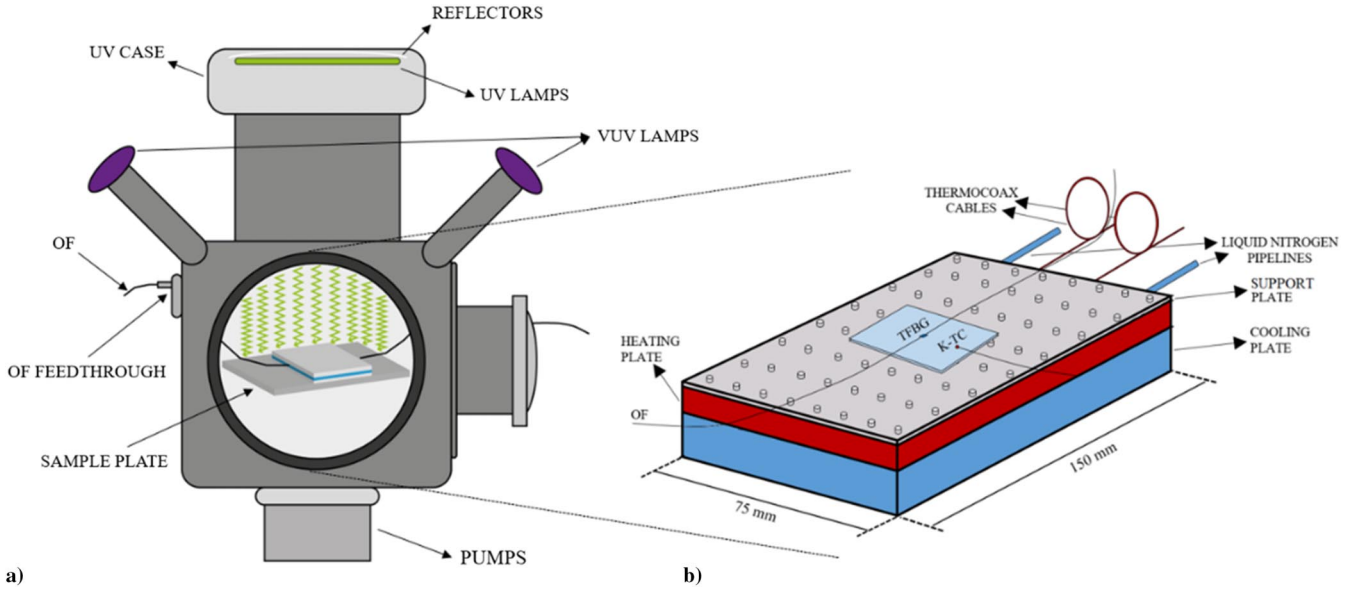

Fig. 5 Schematics of the a) MCross and b) sample plate.

manufacturing. In fact, usually for photosensitive OFs such as the one used here (boron-germanium doped Fibercore PS 1250/1500), the RI core is modulated during FBG production using an UV excimer laser with wavelengths between 193 and 296 nm [23,24]. Hence, considering that the UV radiation from the MCross includes these wavelengths, this may influence or modify the original modulation of the RI core. This would bring unexpected changes in the spectrum of the TFBG during the test, which could lead to erroneous measurements.

To avoid these drawbacks, the TFBGs have been preliminarily tested under UV light to verify their compatibility with the determined operational conditions. As mentioned previously, three kinds of samples were tested: 1) a directly exposed TFBG (Fig. 2, point a), 2) a TFBG covered with a cover glass sheet (Fig. 2, point b), and 3) a TFBG shielded by a Kapton layer (Fig. 2, point c). All the exposures were performed in high vacuum (1.6×10^{-6} mbar, accuracy of the MKS pressure sensor declared by the manufacturer as $\pm 0.5\%$) and with a solar constant of ~ 3. While the lamps were emitting the UV radiation, the TFBGs were connected to the external interrogation system via feedthroughs to acquire and record TFBG transmission spectra during the test. Once the test had been completed, the spectra were processed and analyzed by considering the envelope area of the upper and lower cladding resonance peaks. Hence, the degradation of the TFBG was measured by considering the trend of the envelope area. For this reason, the acquired spectra were demodulated by using the D-T technique that returned the envelope area values, which were normalized with respect to the original area value before the experiment (Figs. 6–8).

The trend of the envelope area in Fig. 6, referred to as the TFBG directly exposed to the UV light, clearly shows a decrease of the envelope area with exposure time. Specifically, at the end of the test, all the resonances in the spectrum of the sensor, analyzed via the envelope area, have resulted in a smaller amplitude than the one at the beginning. If no influence was induced by the UV radiation, they could be expected to have the same area at the end of the test. This means the RI core modulation has undergone a modification due to determined wavelengths of the incident radiation. In particular, because the envelope area (and the spectrum) were reduced (Fig. 9), a possible explanation is that the UV beams are reducing the depth of

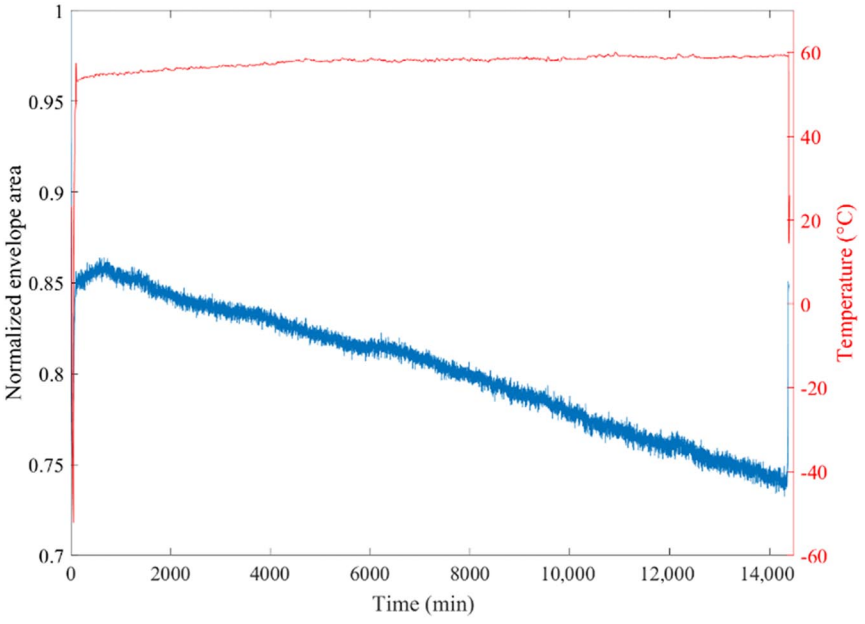

Fig. 6 Normalized envelope area obtained from the directly exposed TFBG.

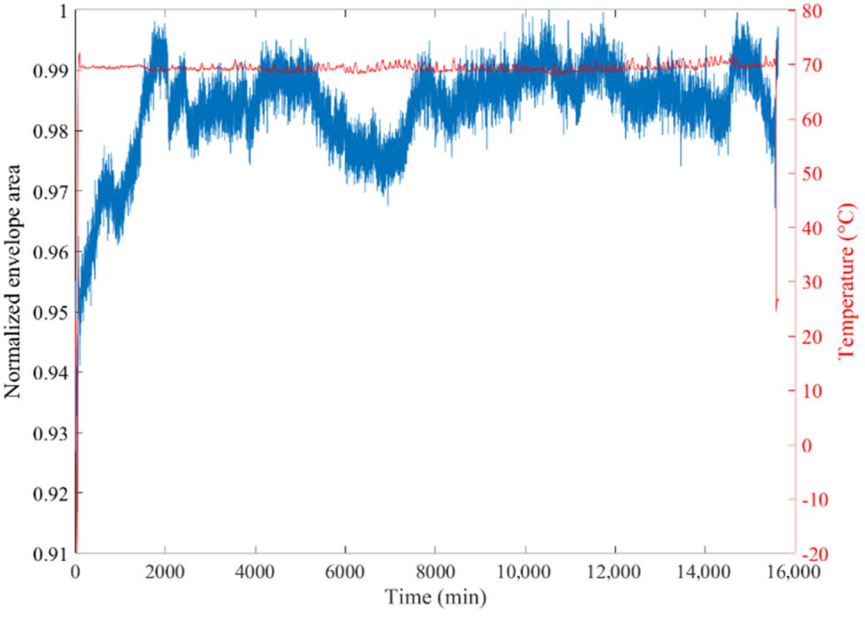

Fig. 7 Normalized envelope area obtained from the TFBG exposed to UV through a cover glass layer.

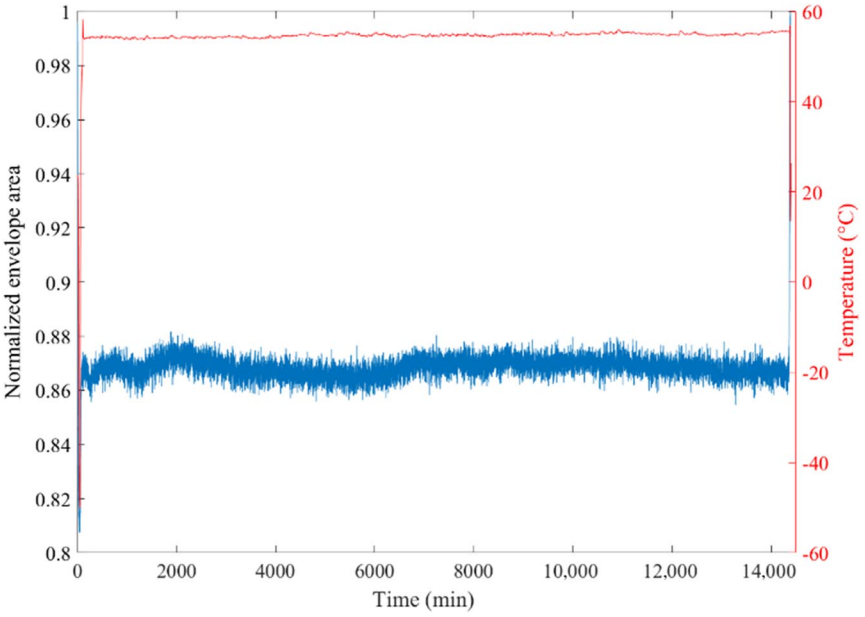

Fig. 8 Normalized envelope area obtained from the TFBG exposed to UV and shielded by the Kapton layer.

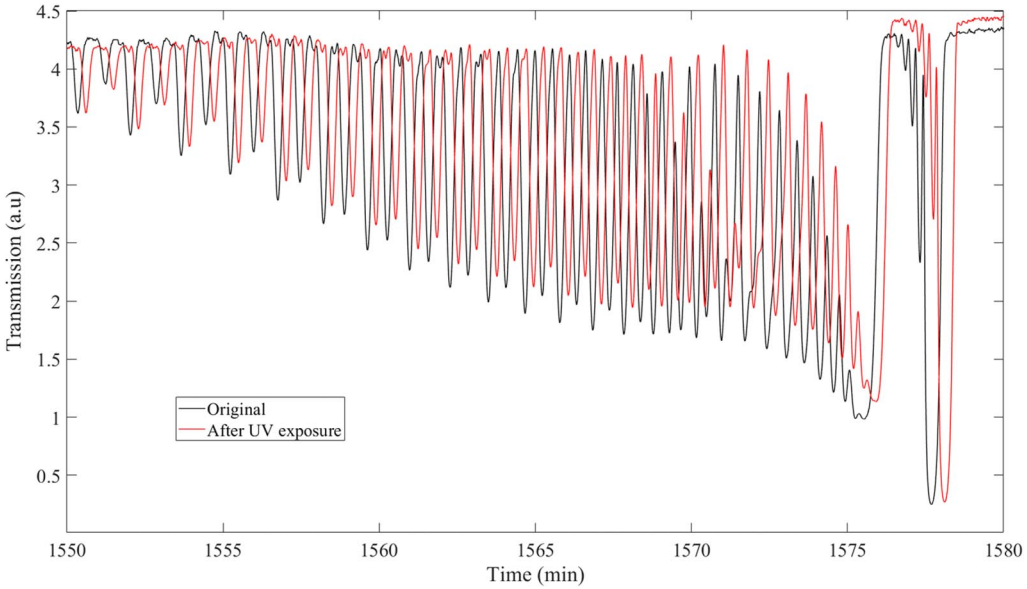

Fig. 9 Comparison between the TFBG transmission spectrum before and after for the bare UV exposure test.

the RI modulation in the OF core created during the TFBG manufacturing. Indeed, this parameter is fundamental to obtain a consistent amplitude of the resonance peaks in the spectrum [25]. Furthermore, as shown in Fig. 9, the comparison between the original and the spectrum after the exposure raises another consequence: all the resonance peaks of the spectrum after the exposure are red-shifted, even while at the same temperature. This could maybe be explained by considering a tensile force induced by the tapes used to hold the OFs; however, because the comparison was made in the absence of external supports (as, for example, clamps), this shift is probably more likely to be due to a change of the original RI core modulation caused by UV radiation.

In the case of the TFBGs shielded by the cover glass (Fig. 7) or the Kapton layer (Fig. 8), the reactions of both sensors to the UV radiation str different from the previous one. In fact, in both cases, the envelope area returns to the original value (or almost, due to the temperature effect [21]) and the original spectra are identical after the UV exposure. This means that the TFBGs were not influenced by the shielding of the layers between themselves and the UV radiation. The reason for this result can be discovered by investigating the wavelengths of the light allowed to pass through the media. Each material possesses an absorption power of light based on its wavelength. Therefore, an Agilent Cary 5000 UV/visible/near-infrared spectrophotometer was used to obtain the percentage of light, along the wavelength range, transmitted through the shielding layers; see Fig. 10.

Figure 10 shows the transmission spectra as a function of the wavelengths. In the case without a shielding layer, the curve referred to is that for the quartz glass that divides the vacuum chamber from the UV case, which transmits all the wavelengths associated with the UV radiation by greater than 90%. Different situations are presented for the case of the cover glass and the Kapton foil. They block the light starting from, respectively, ~340 nm and ~490 nm. In this way, the TFBG internal structure cannot be modified because it is not sensitive to the transmitted wavelengths.

The reason why the Kapton foil was tested with regard to the initial hypothesis to protect the TFBG sensor with a narrow (~150 μm)

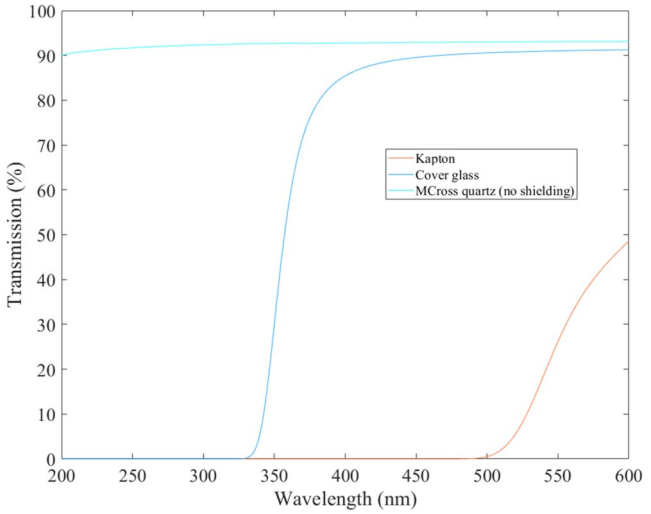

Fig. 10 Transmission percentages of the light through different materials in the range of 200–600 nm.

piece of this material: in case the cover glass was not able to shield the sensor from the radiation. However, because the cover glass protects the TFBG sensor, the sensorized sandwich was realized with the cover glass, as shown in Fig. 11.

VI. UV Effects on Silicone Adhesive Monitored via TFBG Sensor

Once the TFBGs were ready to be embedded, the cover glass sandwich samples were made with the embedded TFBG and TC, as Fig. 3 shows. In this section, the results and discussion are about the effects of UV radiation in vacuum on the silicone adhesive as detected through the simultaneous thermomechanical-refractometric TFBG measurements. Eight samples were tested under the UV lamps, each with increasing ESHs. This value was obtained by multiplying the solar constant by the number of hours of exposure. The TFBG spectra were acquired and then demodulated to calculate the strain–temperature variations and the silicone RI.

In Fig. 12, the strain and temperature variations are reported for a TFBG embedded in a cover glass sandwich and exposed for 808.18 ESHs. Although the TFBGs offer a TR that is much coarser that the

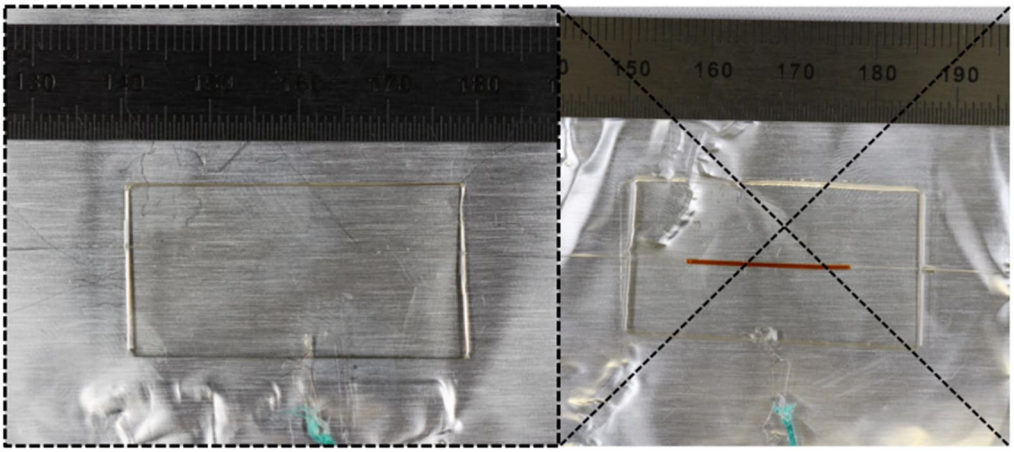

Fig. 11 Configurations of sensorized cover glass sandwich samples.

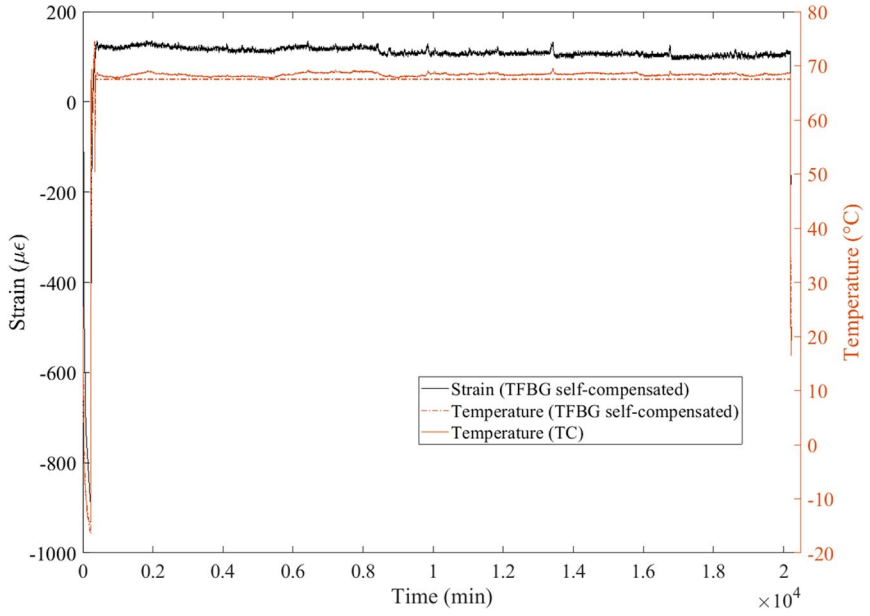

Fig. 12 Thermomechanical measurements performed with the single TFBG and TC temperature trend.

TC, the temperature trend measured by the OF sensor is close to the variation measured by the TC. The maximum difference between the two trends is achieved during the radiation at a constant lamp power. This is due to the TFBG TR, which does not allow small temperature oscillations to be read; however, the maximum difference is ∼2°C, which corresponds to a strain variation of 15 $\mu\varepsilon$. At the beginning of the test, the TFBG measures a significant level of negative strain (reaching to more than -850 $\mu\varepsilon$) due to the slow cooling down caused by the liquid nitrogen cooling plate. Once the lamps are switched on, the strain variation starts to increase, and then the compressive deformation is recovered until reaching a stable value of $\sim +130\ \mu\varepsilon$ in 358th min. From this point, because the TFBG is not able to detect thermal oscillations lower than its resolution, the strain calculation is performed by considering isothermal conditions.

From Fig. 12, it is possible to note some spikes, such as at ∼950th, 13,000th, and 16,500th min and oscillations of the strain levels, which follow the temperature changes detected by the TC. Unfortunately, the TFBG cannot take into account these thermal fluctuations due to its resolution; indeed, the temperature trend measured by the OF sensor is flat. This means the strain measured in this condition is overestimated because part of the wavelength shift that is used to calculate the strain should be compensating thermal variation. The exposure was performed for around 330 h; at the end of the test, once the lamps were switched off, the TFBG measured a final negative deformation of ∼160 $\mu\varepsilon$ at 24.2°C. This means that the UV radiation in high vacuum caused a compressive state inside the silicone adhesive. Thermomechanical measurements can be performed by using this technique on all the samples and in real time; in this way, the state of the material can be detected in any moment of the test.

Simultaneously to the strain–temperature measurements, the refractometric state of the silicone was also evaluated with the embedded TFBG. In particular, the RI depended on many material factors such as the thermal, physical (density), and chemical compositions. Hence, the monitoring of this parameter can provide a global indication of the state of the material. Therefore, the spectra are demodulated to obtain the normalized envelope area, as explained in Sec. II, and the RI is calculated from the fitting correlation function. In Fig. 13, the silicone adhesive RI trend is reported from the spectra of the TFBG previously used for the thermomechanical evaluation.

At the beginning of the experiment, the RI of the silicone adhesive measured by the TFBG was at a value of 1.42506195 (the TFBGs used here have a resolution of $\sim 10^{-8}$). This started to increase when the cover glass sandwich was cooled down by the cooling plate due to the increasing of the elastomer density generated by the negative temperature variation. When the UV lamps were switched on, the temperature increased and the material underwent a positive deformation, which corresponded to a decrease in its density, and consequently a reduction of the RI. However, when a stable range of exposure was achieved, the RI slowly increased during the hours of exposure: the consequence of which could be observed at the end of the exposure. Indeed, when the lamps were switched off, the temperature was redirected with the help of the cooling plate, toward values that were close to the initial values. The silicone RI then decreased; and at the same initial temperature (24.2°C), an RI value of 1.42606481 was determined, which means an RI variation of more than 1×10^{-3} RI with 808.18 ESHs of UV exposure. These measurements were performed on all eight tested samples, which were exposed to the UV radiation with increasing ESHs. Specifically, it was noted that the silicone RI variation was greater the higher the ESH. Therefore, the RI variations of all the cover glass sandwich samples are reported in Fig. 14 with the corresponding ESH values, whereas the values related to the refractometric measurements are reported in Table 1.

In Table 1, the temperatures reported are those recorded at the initial and final refractometric measurements. From Fig. 14, an increase of the RI variation can be observed when increasing the ESHs, and this trend seems to have a good fitting with a linear regression because the resulting square error R^2 of the fitting is 0.92 with a standard deviation of 9.76×10^{-5}. The RI grows from the initial value with increasing ESHs, which means that a longer exposure and/or higher solar constant produces a different physical and/or chemical condition of the material after the radiation and at the same temperature. Specifically, as noted in Ref. [1], the shrinking of the silicone due to the environmental conditions can cause an increase of the RI as the compressive stress compacts the material and increases its density. However, here, the effect of the UV must be taken into account because, although the cover glass can shield part of the UV (Fig. 10), the silicone elastomer absorbs and is photochemically sensitive to the wavelengths of the light passing through [3,5]. For this reason, some chemical reactions may occur inside the silicone due to photoexcitation, which is generated by the radiation. The reactions are favored by the high temperature. The consequences on the adhesive are easily visible and recognizable as the sample undergoes an amber discoloration (Fig. 15), which is more intense the higher the ESH values. Furthermore, this is the main reason for the silicone RI variation that, at this point, may be used as a parameter to detect and evaluate the degradation state of the elastomer during or after the high-vacuum UV exposure. Indeed, a greater RI variation indicates a bigger deviation of the material from its original

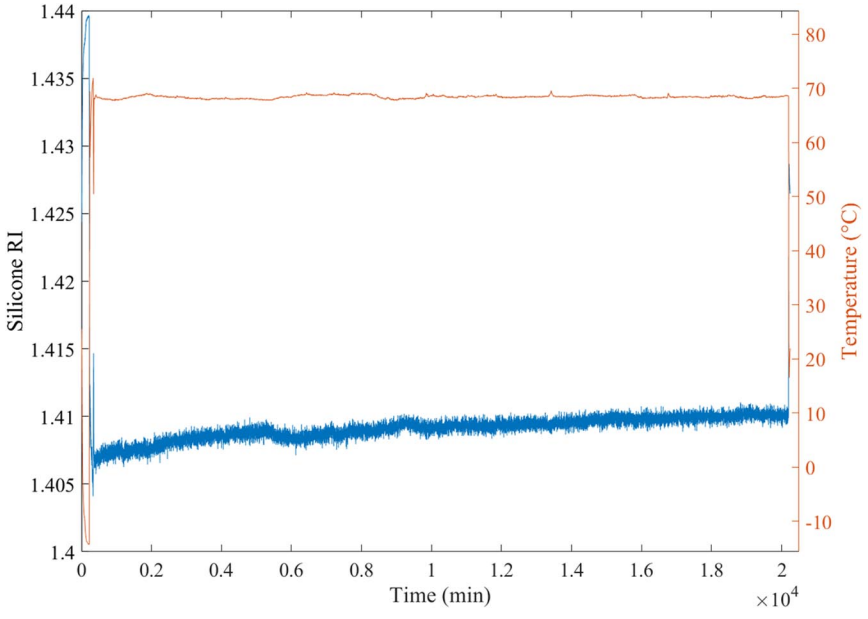

Fig. 13 Silicone RI measurements (blue curve) performed with the embedded TFBG during UV exposure.

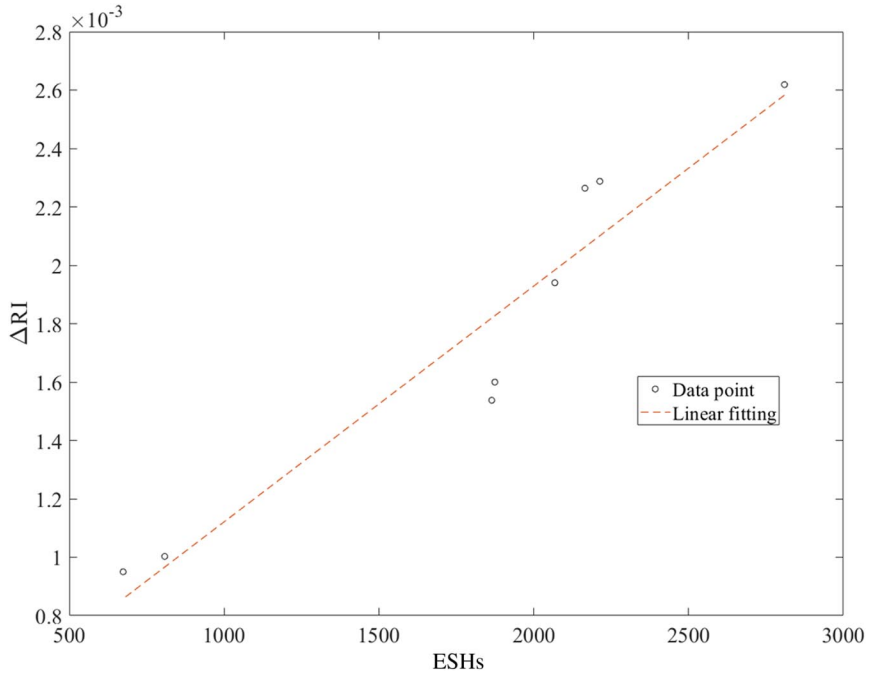

Fig. 14 RI variation of the silicone adhesive of the eight samples tested with increasing ESHs.

Table 1 Values regarding the refractometric measurements

ESHs	Temperature, °C	Initial RI	Final RI	Δ RI (×10^{-3})
2809.75	25.3	1.42439906	1.42701765	2.61859
2213.46	25.4	1.42447117	1.42675870	2.28754
2165.21	24.4	1.42482412	1.42708795	2.26383
2068.16	27.1	1.42383392	1.42577389	1.93997
1874.21	24.5	1.42490283	1.42650266	1.59983
1864.3	24.8	1.42448586	1.42602337	1.53752
808.18	24.2	1.42506195	1.42606481	1.00286
673.89	24.3	1.42479304	1.42574317	0.95013

condition; hence, it may be used as a degradation/aging index of the silicone adhesive.

VII. Sensorized Silicone Adhesive Directly Exposed to UV Radiation

In this section, the results and the discussion regarding the high-vacuum UV exposure of the sample reported in Fig. 4 are described. In this case, one single sample was tested in which the silicone, with an embedded TFBG, was directly exposed to the UV radiation (Fig. 16). The aim of this experiment was to enhance the degradation effects on the silicone adhesive due to the UV radiation, especially regarding the RI variation. The high-vacuum UV exposure was performed for 601.72 h at 5.11 solar constants, which means 3074.79 ESHs of exposure.

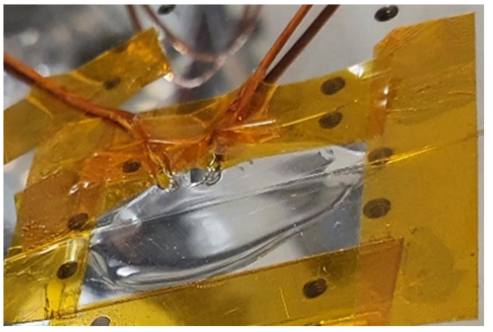

Fig. 16 Sample of silicone directly exposed to the UV radiation on the test plate.

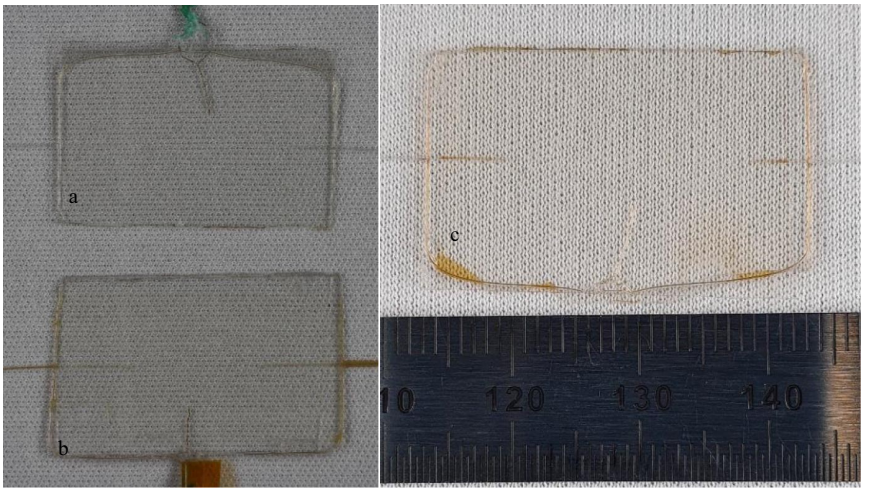

Fig. 15 Inspection of the samples at original state (point a), after 808.18 ESHs (point b), and 2068.16 ESHs of UV exposure (point c).

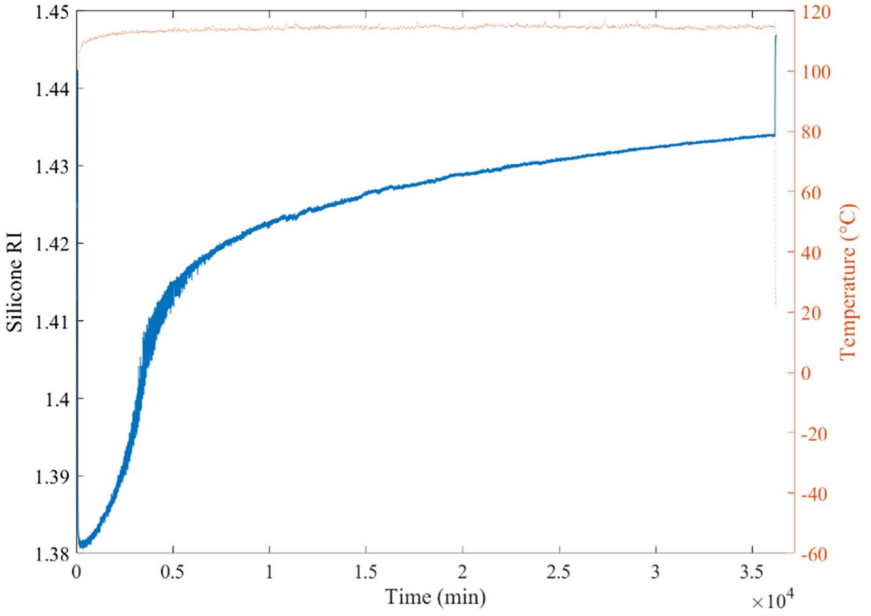

Fig. 17 RI trend of the silicone directly exposed to the UV radiation.

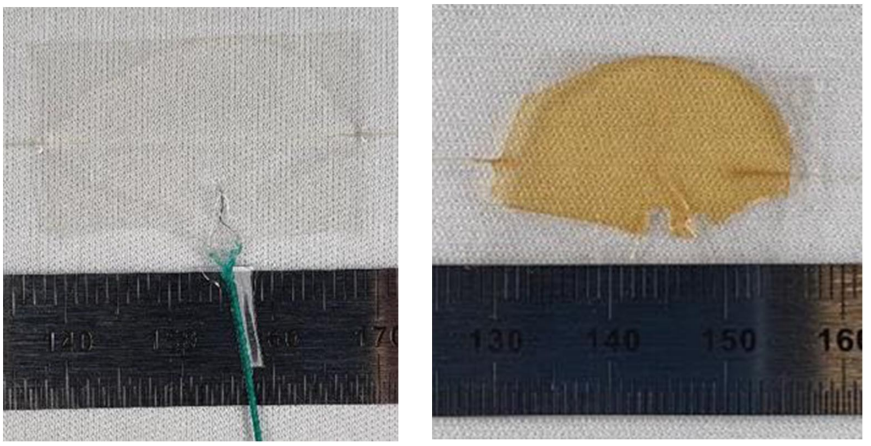

a) **b)**

Fig. 18 Silicone sample a) before and b) after UV exposure.

The silicone RI trend measured by the TFBG is reported in Fig. 17. As previously, the RI changes with the temperature and is higher at the end of the test. This RI increases very higher than the RI variations detected in the previous samples because the lack of the cover glass on top of the sample causes the silicone to absorb a larger wavelength range and amount of UV radiation. A visible consequence of this fact is a stronger discoloration of the sample at the end of the test, as shown in Fig. 18. A comparison between Figs. 18b and point b or point c of Fig. 15 makes evident the stronger effect of the UV on the silicone.

However, although the RI measurements in Fig. 17 performed with the TFBG may seem reliable and reasonable when considering the conditions of samples after the test (Fig. 18b), after a check of the spectra, a degradation of these was noted during the test. The reason is that the silicone adhesive was not able to effectively shield the TFBG as in the case of the cover glass. This was further investigated by performing a UV/visible/near-infrared (NIR) spectroscopy with an Agilent Cary 5000 spectrophotometer on a sample of nonexposed pure silicone adhesive of the same thickness. The transmission spectra are reported in Fig. 19.

From Fig. 19, it is clear that the tested silicone lets a broader bandwidth of UV light pass in comparison to the cover glass and

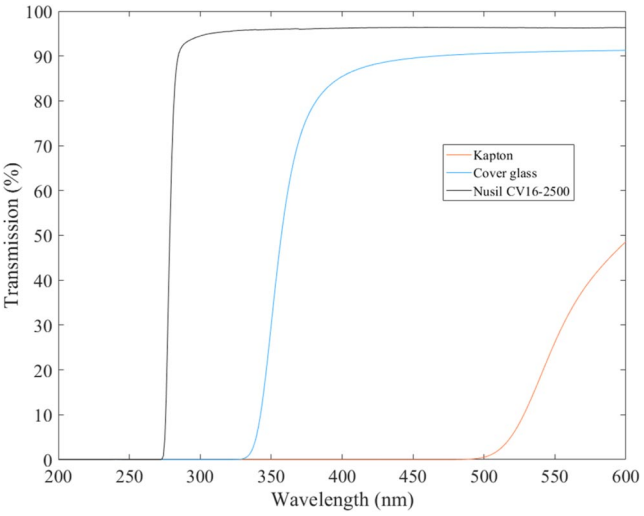

Fig. 19 Transmission light spectrum through NuSil CV16-2500 with those of cover glass and Kapton.

Kapton foil. These wavelengths may influence the RI core modulation inside the OF, and this is clearly detected in the TFBG spectra: the consequences of which are similar to those reported in Fig. 9. This makes the TFBG measurements not reliable at this stage.

However, the TFBG spectra can be exploited by performing a compensation of the TFBG spectra using the decay trend of the bare TFBG under UV light (Fig. 6) and the transmission light spectrum of the silicone adhesive sample tested in the spectrophotometer before and after the UV exposure (Fig. 20). Specifically, from the ratio of the areas obtained by performing the integral of the transmission curves in Fig. 20, the transmission decay percentage trend of the silicone adhesive can be calculated at the end of the experiment in the wavelength range of 200–400 nm with respect to its initial condition. Considering the starting transmission to be 100%, this results in decay to 20.92% at the end of the exposure. At this point, by supposing a linear decay rate of the silicone transmission and taking into account the linear decrease of the envelope area due to UV in air along the exposure time (Fig. 6), a compensation can be applied on this latter trend by considering the decreasing silicone transmission of the UV light at each moment of the exposure. The linear trend of the percentage of the NuSil transmission is described from the following equation:

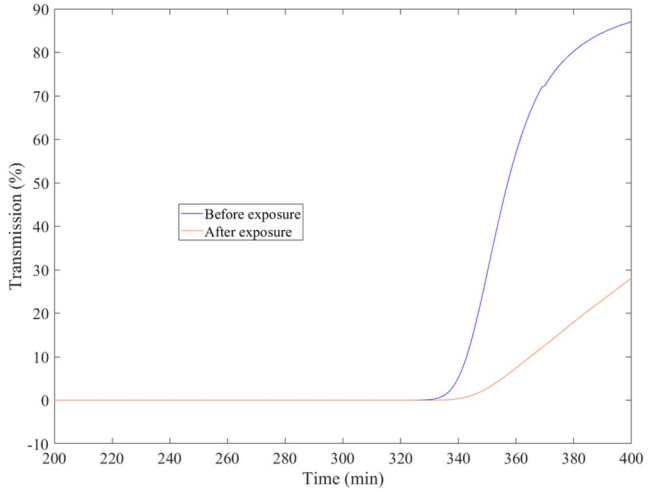

Fig. 20 Transmission light spectrum through the silicone adhesive sample (Fig. 18) before and after UV exposure.

$$P(\mathrm{ESH}) = at + b \tag{2}$$

where coefficients a and b depend on the linear fitting. The decay percentage P depends on the equivalent solar hour (ESH) minute at which it is calculated and can be written respect to this unit. In the same way, the linear trend of the envelope area can be obtained, and hence its percentage of decay along the exposure time.

The NuSil decay variation is then obtained as $P_{\mathrm{var}} = 1 - P$. Hence, the shielding effect of the silicone can be introduced on the envelope area trend and a new linear fitting function describing the degradation of the envelope area due to the UV radiation but partially protected by the silicone adhesive can be found. This process is made by calculating the compensated decay of the envelope area:

$$P_{\mathrm{comp}} = P_{\mathrm{Area}} \times P_{\mathrm{var}} \tag{3}$$

where P_{Area} is the unitary envelope area decay obtain at each moment of the exposure from the linear fitting between the initial area and the final area after the exposure over the testing time. Hence, successively, the compensated unitary envelope area variation is obtained:

$$P_a = P_{\mathrm{var}} - P_{\mathrm{comp}} \tag{4}$$

for which value is used to calculate the variation of the envelope area:

$$A_{\mathrm{var}} = A \times P_a \tag{5}$$

Therefore, at the end, the compensated area A_{new} value by using the noncompensated area value A added with the variation A_{var} from the compensation.

At this point, the envelope areas from the spectra of the sample used for the refractometric measurements of the silicone sample (Fig. 17), are corrected and a new RI trend for the silicone is calculated, and this is reported in Fig. 21.

The compensation of the RI measurements allowed the degradation effects on the cladding envelope area to be isolated and removed from those caused by the RI variation of the surrounding environment. Although the compensation reduced the positive RI variation measured by the TFBG, it is still possible to detect a consistent variation with respect to the initial value, as Fig. 21 shows. In particular, at 24.2°C, an initial RI of ∼1.424 was measured, corresponding to the sample in Fig. 18a; whereas after the UV exposure, the final RI measured was ∼1.440 at the same temperature, which is a variation of 1.6×10^{-2} (around one order bigger than the RI variation reported in Table 1). This underlines that the TFBG refractometric

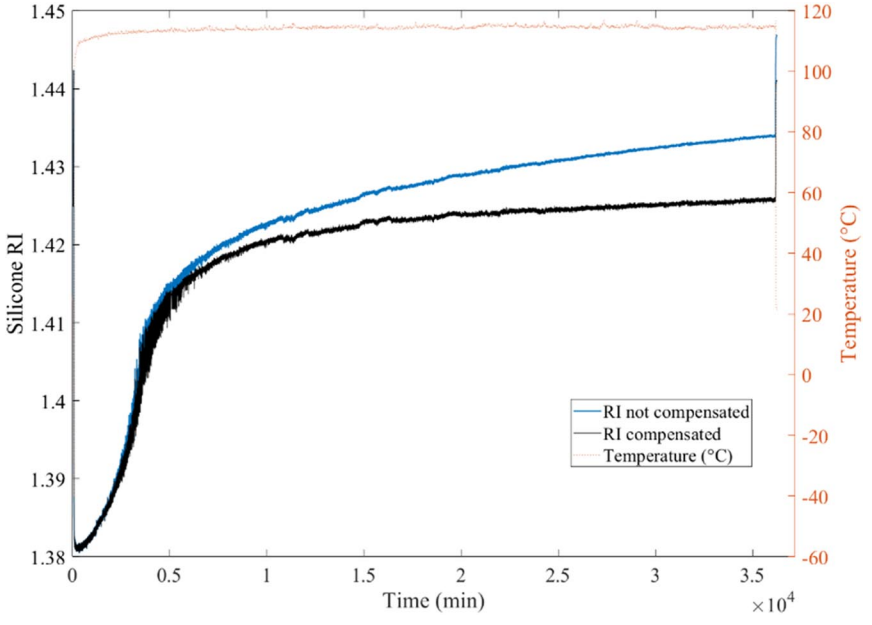

Fig. 21 Silicone RI measurements performed with the TFBG spectra with compensated UV degradation.

measurements can detect the operational conditions of the material and the evolution of its degradation during harsh working environmental conditions.

VIII. Conclusions

In this work, TFBG sensors have been demonstrated to be able to detect the thermomechanical and refractometric states of a silicone adhesive, which is used to bound two thin cover glasses, during a simulated space environmental test characterized by high vacuum and UV exposure. First of all, the TFBGs were tested under UV light to prove their performance in working under the testing conditions. It was necessary to shield the OF sensors with at least a cover glass to avoid the degradation of the spectrum during the measurements. This condition perfectly fit the subsequent test methodology where each TFBG was embedded in the silicone between the cover glasses.

Then, several cover glass sandwiches were exposed in high vacuum and under UV radiation for different times; in the meantime, the spectra of each TFBG were acquired. Through the demodulation of the spectra, the thermomechanical variations and the RI of the material were measured along the entire testing time. Specifically, a substantial level of negative deformation ($\sim$160 $\mu\varepsilon$) after the test was found, which means a shrinking of the material due to the outgassing and radiation. The RI measurements also reported interesting information on the material state. Indeed, the D-T demodulation allowed the silicone RI value of all the samples during the test time to be obtained. In particular, an increasing RI variation was calculated with an increase of the ESH value, which means with the harshness of the testing conditions (solar constant and/or exposure time). This proved the ability of the TFBG to monitor and detect the state of the material based on its operational conditions. Specifically, the detected silicone RI variations were from $\sim 0.95 \times 10^{-3}$ RI for 673.89 ESHs until $\sim 2.62 \times 10^{-3}$ RI at 2809.75 ESHs, following a linear line.

A further experiment was performed on a sample of TFBG sensorized silicone adhesive directly exposed to the UV radiation without the shielding of the top cover glass. This experiment aimed at enhancing the effects of the radiation on the silicone to investigate the reaction of the TFBG to more severe damage. The consequence was the necessity to perform a compensation of the TFBG spectrum to remove the sensor degradation due to the UV beams from its spectrum and to obtain the RI values. This compensation was achieved by exploiting the light transmission percentages obtained with the UV/visible/NIR spectrophotometer testing on the silicone sample before and after the UV exposure, as well as by finding the linear degradation trend of the cladding envelope area in the TFBG spectrum. In this way, a reliable RI variation of 1.6×10^{-2} RI was found along $\sim$3074 ESHs of exposure. The substantial Δ RI difference of one order of magnitude between the longest tested cover glass sandwich sample and the directly exposed silicone sample (with similar exposure time) demonstrates two aspects: the shielding effect of the cover glass, and the ability of the TFBG to detect the degradation state of the material.

In conclusion, the TFBG sensors were demonstrated to be a potential valid solution for in situ sensing of space-qualified polymers, as in the case of the silicone adhesive used in the solar arrays. These sensors are minimally intrusive, compatible with operating in a space environment, and provide reliable measurements useful for the monitoring of the thermomechanical and refractometric states of the material during its operations in a space environment.

Future research might be focused on the correlation between the RI variation occurring in the silicone during the UV exposure and the thermal optical properties of the silicone adhesive.

Acknowledgments

This research was supported by the ESA's European Space Research and Technology Center (Visiting Researcher Programme) and the Operationeel Programma Zuid-Nederland Project as part of the Dutch Composite Maintenance Centre, which is supported by the Europees Fonds voor Regionale Ontwikkeling and the North Brabant province of the Netherlands. The views expressed herein can in no way be taken to reflect the official opinion of the European Space Agency and are not intended to endorse particular technologies, companies, or products.

References

[1] Fazzi, L., Dias, N., Holynska, M., Tighe, A. P., Rampini, R., and Groves, R. M., "Monitoring of Silicone Adhesive in Space Solar Cells with an Embedded Multi-Parameter TFBG Sensor in a Simulated Space Environment," *Measurement Science and Technology Journal*, Vol. 33, No. 8, 2022, Paper 085108. https://doi.org/10.1088/1361-6501/ac6d45

[2] Kutz, M., *Handbook of Environmental Degradation of Materials*, William Andrew Publ., Oxford, England, U.K., 2008, Chap. 23.

[3] Zimmermann, C. G., "On the Kinetics of Photodegradation in Transparent Silicones," *Journal of Applied Physics*, Vol. 103, No. 8, 2008, Paper 083547. https://doi.org/10.1063/1.2891243

[4] Tribble, A. C., *The Space Environment: Implications for Spacecraft Design*, Princeton Univ. Press, Princeton, NJ, 1995.

[5] Fischer, H. R., Semprimoschnig, C., Mooney, C., Rohr, T., van Eck, E. R. H., and Verkuijlen, M. H. W., "Degradation Mechanism of Silicone Glues Under UV Irradiation and Options for Designing Materials with Increased Stability," *Polymer Degradation and Stability*, Vol. 98, No. 3, 2013, pp. 720–726. https://doi.org/10.1016/j.polymdegradstab.2012.12.022

[6] Schnabel, W., *Polymer Degradation: Principles and Practical Applications*, Macmillan, New York, 1981, Chap. 4.

[7] Banks, B. A., Rutledge, S. K., Sechkar, E., Stueber, T., Snyder, A., de Groh, K. K., Haytas, C., and Brinker, D., "Issues Effects of Atomic Oxygen Interactions with Silicone Contamination on Spacecraft in Low Earth Orbit," *Proceedings of the 8th International Symposium on Materials in a Space Environment, 5th International Conference on Protection of Materials and Structures from the LEO Space Environment*, France, 2000.

[8] Edwards, D. L., Tighe, A. P., Van Eesbeek, M., Kimoto, Y., and de Groh, K. K., "Overview of the Natural Space Environment and ESA, JAXA, and NASA Materials Flight Experiments," *MRS Bulletin*, Vol. 35, No. 1, 2010, pp. 25–34. https://doi.org/10.1557/mrs2010.613

[9] Claus, R. O., Murphy, K. A., and Bennett, K. D., "Smart Skins and Structures Overview," *Proceedings of the SEM Spring Conference on Experimental Mechanics, A91-16751*, 04-39, 1989, pp. 528–533.

[10] Rogowski, R. S., Heyman, J. S., and Holben, M. S., Jr., "Sensor Technology for Smart Structures," *Proceedings of the International Instrumentation Symposium, A91-1965106-35*, 1989, pp. 177–181.

[11] Rogowski, R. S., "On-Orbit Structural Health Monitoring," *Proceedings of the SPIE*, Vol. 1370, Fiber Optic Smart Structures and Skins III, SPIE, Bellingham, WA, Dec. 1990. https://doi.org/10.1117/12.24829

[12] Aggarwal, M. D., Penn, B. G., and Miller, J., "Triboluminescent Materials for Smart Optical Damage Sensors for Space Applications," NASA TM-2008-215410, 2008.

[13] Hang, S. G., Kang, D. H., and Kim, C. G., "Real-Time Monitoring of Transverse Thermal Strain of Carbon Fiber Reinforced Composites Under Long-Term Space Environment Using Fiber Optic Sensors," *NDT & E International*, Vol. 42, No. 5, 2009, pp. 361–368. https://doi.org/10.1016/j.ndteint.2009.01.001

[14] Osei, A. J., "Monitoring of Structural Integrity of Composite Structures by Embedded Optical Fiber Sensors," *Journal of Emerging Trends in Engineering and Applied Sciences*, Vol. 5, No. 7, 2014, pp. 101–105. https://doi.org/10520/EJC156929

[15] Savill, T., and Jewell, E., "Techniques for In Situ Monitoring the Performance of Organic Coatings and Their Applicability to the Pre-Finished Steel Industry: A Review," *Sensors*, Vol. 21, No. 9, 2021, Paper 6334. https://doi.org/10.3390/s21196334

[16] Hufenbach, B., Habinc, S., and Vuilleumier, P., "Space Applications for Smart Sensors," *European Space Agency, Proceedings of the Eurosensors XIII, 13th European Conference on Solid-State Transducers*, 1999.

[17] Dumstorff, G., Paul, S., and Lang, W., "Integration Without Disruption: The Basic Challenge of Sensor Integration," *IEEE Sensors Journal*, Vol. 14, No. 7, 2014, pp. 2102–2111. https://doi.org/10.1109/JSEN.2013.2294626

[18] Fazzi, L., Struzziero, G., Dransfeld, C., and Groves, R. M., "A Single Three-Parameter Tilted Fibre Bragg Grating Sensor to Monitor the Thermosetting Composite Curing Process," *Polymer and Composites*, Vol. 8, No. 1, 2022, pp. 33–41. https://doi.org/10.1080/20550340.2022.2041221

[19] Fazzi, L., and Groves, R. M., "Demodulation of a Tilted Fibre Bragg Grating Transmission Signal Using α-Shape Modified Delaunay Triangulation," *Measurement*, Vol. 166, Dec. 2020, Paper 108197. https://doi.org/10.1016/j.measurement.2020.108197

[20] Fazzi, L., Valvano, S., Alaimo, A., and Groves, R. M., "A Simultaneous Dual-Parameter Optical Fibre Single Sensor Embedded in a Glass Fibre/Epoxy Composite," *Composite Structures*, Vol. 270, Dec. 2021, Paper 114087. https://doi.org/10.1016/j.compstruct.2021.114087

[21] Fazzi, L., and Groves, R. M., "Refractometric Properties of a TFBG Sensor Demodulated Using α-Shape Modified Delaunay Triangulation," *Optics*, Vol. 2, No. 2, 2021, p. 113–133. https://doi.org/10.3390/opt2020012

[22] "Space Environment," European Cooperation for Space Standardization STD ECSS-E-ST-10-04c, 15 June 2020.

[23] Singh, N., Jain, S. C., Aggarwal, A. K., and Bajpai, R. P., "Fibre Bragg Grating Writing Using Phase Mask Technology," *Journal of Scientific and Industrial Research*, Vol. 64, Feb. 2005, pp. 108–115.

[24] Hu, X., Liu, Y., Jiang, J., Lin, W., Qu, H., and Caucheteur, C., "Tilted Fiber Bragg Grating Inscription in Boron Co-Doped Photosensitive Optical Fiber Using 266 nm Solid State Laser Pulses," *IEEE Sensors Journal*, Vol. 22, No. 3, 2022, pp. 2229–2236. https://doi.org/10.1109/JSEN.2021.3137249

[25] Erdogan, T., "Fiber Grating Spectra," *Journal of Lightwave Technology*, Vol. 15, No. 8, 1997, pp. 1277–1294. https://doi.org/10.1109/50.618322

M. L. Walker
Associate Editor